Effect of helicity on the effective diffusivity for incompressible random flows

D. S. Dean

Laboratoire de Physique Quantique, l'Institut de Recherche Sur les Systemes Atomiques et Moléculaires Complexes,
Université Paul Sabatier, 118 route de Narbonne, 31062 Toulouse Cedex, France

I. T. Drummond and R. R. Horgan

Department of Applied Mathematics and Theoretical Physics, Centre for Mathematical Sciences,
University of Cambridge, Wilberforce Road, Cambridge CB3 0WA, United Kingdom

The advection of a passive scalar by a quenched (frozen) incompressible velocity field is studied by extensive high precision numerical simulation and various approximation schemes. We show that second-order self-consistent perturbation theory, in the absence of helicity, perfectly predicts the effective diffusivity of a tracer particle in such a field. In the presence of helicity in the flow, simulations reveal an unexpectedly strong enhancement of the effective diffusivity which is highly nonperturbative and most visible when the bare molecular diffusivity of the particle is small. We develop and analyze a series of approximation schemes which indicate that this enhancement of the diffusivity is due to a second order effect, whereby the helical component of the field, which does not directly renormalize the effective diffusivity, enhances the strength of the nonhelical part of the flow, which in turn renormalizes the molecular diffusivity. We show that this renormalization is most important at a low bare molecular diffusivity, in agreement with numerical simulations.

I. INTRODUCTION

The advection of passive fields, subject to molecular diffusion and convection by turbulent fluid, has been extensively studied by both theoretical and computational techniques [1–6]. By comparing the results of simulation with the theoretical prediction for various long-range quantities, the efficacy of the theoretical methods can be tested, albeit in somewhat artificial models. The applications to the physics of complex systems and engineering are manyfold. In practical problems we need to calculate the bulk properties of random media given statistical models for the disorder present. In general, the complexity of these real world problems means that one must resort to approximation schemes to calculate these large-scale bulk properties. It is therefore essential to verify various methods of analysis on model problems before one can be confident that these or similar methods can be applied to more realistic systems. The success of an approach depends on whether the approximation preserves the essence of the physical mechanism responsible for determining the long-range parameters of the advection in terms of the parameters describing the local characteristics of the flow. In this paper we consider advection in a helical Gaussian turbulent flow, which was originally studied in Ref. [4]. The surprising result, observed on the basis of simulation, is that the long-range effective diffusivity κ_e is greatly enhanced by the presence of the helicity by more than a factor of 2, the effect being strongest for a small molecular diffusivity κ_0. In the absence of helicity the calculation of κ_e to two loops in self-consistent perturbation theory agrees accurately with the simulation for all κ_0. However, such an approach predicts that even maximal helicity will have only a small effect of the order of 10%. This is in stark contrast to the results of simulation. The puzzle is to explain these results for what is a relatively simply posed system. A success-

ful theoretical approach will involve infinite resummations of contributions, and it is in this sense that the enhancement is nonperturbative.

In this paper we discuss a possible resolution of the conflict between theory and simulation by using various methods to identify the low-wave-number effective theory governing the diffusive dispersal of particles advected in the turbulent flow when helicity is present. The derivation of the effective theory is guided by the renormalization group (RG) idea that the Green function at low wave number is, in some approximation, the solution to an effective second-order differential equation whose parameters are determined self-consistently in terms of the original or ''bare'' defining the model. The effect of helicity in the flow causes the turbulent velocity field $\mathbf{u}(\mathbf{x},t)$ to be additively renormalized by a term proportional to the vorticity, $\boldsymbol{\omega} = \boldsymbol{\nabla} \times \mathbf{u}$. The coefficient of proportionality is a pseudoscalar which is generated by the axial-vector nature of the helical flow and so depends on the helicity h, defined in terms of u by

$$h = \langle \mathbf{u} \cdot \boldsymbol{\nabla} \times \mathbf{u} \rangle, \tag{1.1}$$

where $\langle \cdot \rangle$ denotes the ensemble average over the random velocity field. In our model the magnitude of h is measured by a parameter λ, $0 \leq \lambda \leq 1$, and the results are given in terms of λ. The usual perturbative result for the dependence of κ_e on λ is that κ_e is a series in λ^2 for all values of κ_0. This is self-evident since the magnitude of κ_e is independent of the sign of λ. The simulation is seemingly consistent with this fact for $\lambda < 0.2$ at $\kappa_0 = 0$ but is not well fitted by any simple approach, and for larger λ the curve lies far higher than the naive calculation. We discuss an improved self-consistent scheme which expresses the Green function and vertex functions as solutions to integral equations which are solved in a low-wave-number approximation. This method leads to a strong enhancement of κ_e for increasing λ and, as such, is a good indication that we are on the right track. However, for small λ the effect is paradoxically too strong, leading to a

nonanalytic dependence of κ_e on λ which is predicted to be $\kappa_e \sim \lambda^{2/3}$ in the one-loop case. This is possibly due to the approximation made in obtaining the solution, but it is a complex matter to ascertain whether this is so. An alternative approach is to use the functional Hartree-Fock method, which leads to an integral equation for the Green function self-energy as a function of wave number. The result of this method for $\kappa_e(\lambda)$ is better behaved at small λ, but the predicted enhancement is not large enough and does not fit the simulation data. In general, the effect is most pronounced for small κ_0, and empirically from our simulation we find that the results distinguish the regions $\kappa_0 \ll 0.2$ and $\kappa_0 \gg 0.2$. There is a pronounced dip in κ_e vs κ_0 at $\kappa_0 \sim 0.2$ for $\lambda = 1$. This dip is not predicted by either of the methods mentioned so far.

We also present a renormalization group approach which shows a mechanism for the enhancing effect of helicity on κ_e. The renormalization group is normally most useful for computing anomalous exponents, since they are generally independent of much of the details defining the model: the idea of universality. It is much more difficult to control a standard RG analysis if it is used to calculate the coefficients of scaling behavior, i.e., observables like κ_e. However, in Ref. [7] we reported on a successful use of the RG in predicting κ_e for gradient flows, and we believe that an RG analysis can generally give a strong indication of the kind of mechanism which influences the size of parameters controlling the large-scale characteristics of advection. In this paper we show that the flow at large wave vector can strongly enhance κ_e when κ_0 is small. In particular, this approach does provide a mechanism for the dip observed in κ_e vs κ_0 at $\kappa_0 \sim 0.2$ for $\lambda = 1$.

In Sec. II the model and the formalism are reviewed. In Sec. III the perturbation theory is briefly described. In Sec. IV the self-consistent integral equations for the Green function and vertex functions are derived to one-loop, and the small wave vector approximation for κ_e is derived. In Sec. V the functional Hartree-Fock method is examined. In Sec. VI the renormalization group approach is explained. In Sec. VII the conclusions are presented.

II. MODEL AND FORMALISM

In Ref. [4] the problem of a passive scalar advected by an incompressible turbulent flow with a molecular diffusivity was studied. The turbulent fluid velocity field $\mathbf{u}(\mathbf{x},t)$ was described by its statistical properties which were assumed to be Gaussian, and so fully determined by the velocity autocorrelation function. In the original study the flow was time dependent, but since the enhancement of κ_e by helicity in the flow is also present for time-independent flows, we assume here, for simplicity, a time-independent flow (i.e., quenched or frozen turbulence) for which the autocorrelation function can be expressed in the following form:

$$\langle u_i(\mathbf{x}) u_j(\mathbf{x}') \rangle = \int \frac{d^3 k}{(2\pi)^3} e^{i\mathbf{k}\cdot(\mathbf{x}-\mathbf{x}')} F_{ij}(\mathbf{k}). \quad (2.1)$$

The ensemble of velocity fields was taken to be homogeneous and isotropic, and so for incompressible fluids $F_{ij}(\mathbf{k})$ can be written as

$$F_{ij}(\mathbf{k}) = \Phi(\mathbf{k})(k^2 \delta_{ij} - k_i k_j) + \Psi(\mathbf{k}) i \epsilon_{imj} k_m, \quad (2.2)$$

where Ψ represents the presence of helicity in the flow. In Ref. [4] it was assumed that Φ and Ψ took the factorized forms

$$\Phi(\mathbf{k}) = \frac{(2\pi)^3}{3} A^2 E(k),$$

$$\Psi(\mathbf{k}) = \frac{(2\pi)^3}{3} A^2 k E(k) \sin 2\psi, \quad (2.3)$$

where A is chosen so that

$$\int d\mathbf{k} E(k) = 1, \quad \langle \mathbf{u}\cdot\mathbf{u} \rangle = u_0^2, \quad (2.4)$$

and where u_0 is the rms velocity. Choosing the angle ψ to be k independent means that the helicity is of equal strength at all wave vectors. The helicity parameter h is been defined in Eq. (1.1), and with the definitions in Eq. (2.3), we find

$$h = \frac{2}{3} A^2 \langle k^3 \rangle \sin 2\psi, \quad (2.5)$$

where $\langle k^3 \rangle$ is the expectation value with respect to the distribution $E(k)$. The passive scalar field $\Theta(\mathbf{x},t)$ is advected according to the equation

$$\frac{d\Theta}{dt} = \kappa_0 \nabla^2 \Theta - \boldsymbol{\nabla}\cdot(\mathbf{u}\Theta), \quad (2.6)$$

and the effective, or long-range, diffusivity κ_e is defined by

$$\langle \mathbf{x}\cdot\mathbf{x} \rangle(t) = \left\langle \int d^3 x \mathbf{x}\cdot\mathbf{x}\Theta(\mathbf{x},t) \right\rangle,$$

$$= 6\kappa_e t + O(t^0) \quad \text{as} \quad t\to\infty, \quad (2.7)$$

where Θ is normalized to unity:

$$\int d^3 x \Theta(\mathbf{x},t) = 1. \quad (2.8)$$

For the purposes of numerical simulation a particular member of the velocity-field ensemble is then realized by [1,2,4]

$$\mathbf{u}(\mathbf{x}) = A \sum_{n=1}^{N} \{ (\boldsymbol{\xi}_n \cos\psi - \boldsymbol{\chi}_n \times \hat{\mathbf{k}}_n \sin\psi) \times \mathbf{k}_n \cos(\mathbf{k}_n\cdot\mathbf{x})$$

$$+ (\boldsymbol{\chi}_n \cos\psi + \boldsymbol{\xi}_n \times \hat{\mathbf{k}}_n \sin\psi) \times \mathbf{k}_n \sin(\mathbf{k}_n\cdot\mathbf{x}) \}, \quad (2.9)$$

where the vectors $\boldsymbol{\xi}_n$ and $\boldsymbol{\chi}_n$ are distributed uniformly and independently over the unit sphere and the wave vector $\mathbf{k}_n$ is distributed according to the distribution $E(k)$. For N sufficiently large the central limit theorem guarantees that $\mathbf{u}(\mathbf{x})$ is

Gaussian up to $O(1/N)$ corrections. We have used $N=64$, for which these effects are sufficiently small for our purposes.

To simulate the evolution of the scalar field $\Theta(\mathbf{x},t)$, we numerically integrate the stochastic equation for the evolution of a particle with path $\mathbf{x}(t)$ given by

$$\dot{\mathbf{x}}(t)=\mathbf{u}(\mathbf{x}(t))+\boldsymbol{\eta}(t), \tag{2.10}$$

where $\boldsymbol{\eta}(t)$ is a Gaussian random variable with $\langle\boldsymbol{\eta}(t)\rangle=\mathbf{0}$ and $\langle\boldsymbol{\eta}(t)\cdot\boldsymbol{\eta}(t')\rangle=2\kappa_0\delta(t-t')$. The resulting probability distribution for particle position $\mathbf{x}(t)$ is then $\Theta(\mathbf{x},t)$ with the initial condition $\Theta(\mathbf{x},0)=\delta(\mathbf{x})$.

The discrete form of Eq. (2.10), suitable for numerical integration, is

$$\mathbf{x}_{n+1}-\mathbf{x}_n=\mathbf{u}(\mathbf{x}_n)\Delta t+(2\kappa_0\Delta t)^{1/2}\boldsymbol{\epsilon}_n, \tag{2.11}$$

where $\boldsymbol{\epsilon}_n$ is a Gaussian random 3 vector of zero mean and unit variance for each component. This equation models Eq. (2.10) correctly to $O(\Delta t)$, but the details of a third-order Runge-Kutta scheme correct to $O(\Delta t^3)$ were given in Ref. [4]. We use this third-order scheme in our numerical simulation.

The effective diffusivity κ_e is then computed from the ensemble of paths by

$$\langle\mathbf{x}(t)\cdot\mathbf{x}(t)\rangle_{\text{paths}}=\lim_{M\to\infty}\frac{1}{M}\sum_{a=1}^{M}\mathbf{x}^{(a)}(t)\cdot\mathbf{x}^{(a)}(t),$$

$$=6\kappa_e t+O(1)\quad\text{as}\quad t\to\infty. \tag{2.12}$$

Here M is the total number of paths averaged over, and (a) labels the member of the ensemble of paths. In practice, M is finite but large enough to give an estimate of κ_e with small error. In addition, t must be large enough so that the path evolution is in the asymptotic regime where the evolution can be suitably described in terms of long-range effective, or "renormalized" quantities. That t is large enough is tested by ensuring that the estimate for κ_e is independent of t within statistical errors.

III. PERTURBATION THEORY

The perturbative approach to solving Eq. (2.6) is well known [8,9,6], and we only summarize the necessary results here. Since we are interested in the effective parameters governing the evolution of the distribution $\Theta(\mathbf{x},t)$, we study the related Green function $G(\mathbf{x})$, which satisfies

$$\kappa_0\nabla^2 G-\mathbf{u}\cdot\nabla G=-\delta(\mathbf{x}), \tag{3.1}$$

where the incompressibility of u has been used. A perturbation series in $\mathbf{u}/\kappa_0$ for $\tilde{G}(\mathbf{k})$ can be generated by iterating the formal solution to Eq. (3.1) in Fourier space:

$$\tilde{G}(\mathbf{k})=\frac{1}{\kappa_0 k^2}+\frac{1}{\kappa_0 k^2}\int\frac{d\mathbf{q}}{(2\pi)^3}i(\mathbf{k}-\mathbf{q})\cdot\tilde{\mathbf{u}}(\mathbf{q})\tilde{G}(\mathbf{k}-\mathbf{q}). \tag{3.2}$$
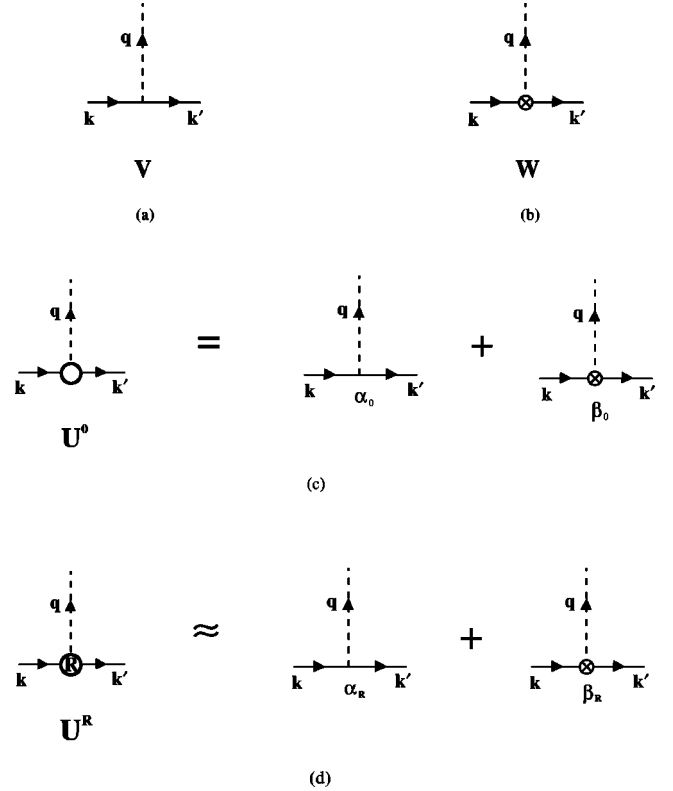

FIG. 1. The vertices occurring in the perturbation schemes: (a) The primitive velocity field vertex. (b) The primitive vorticity vertex. (c) The bare complete vertex of the effective diffusion equation. (d) The renormalized complete vertex approximated as a sum of renormalized vertices associated with the velocity field and the vorticity.

The Green function averaged over the velocity ensemble, $\langle\tilde{G}(\mathbf{k})\rangle$, can then be written as

$$\langle\tilde{G}(\mathbf{k})\rangle=\frac{1}{\kappa_0 k^2-\Sigma(\mathbf{k})}, \tag{3.3}$$

where the averaging over the velocity ensemble is done using Wicks theorem to give a diagrammatic expansion, and $\Sigma(\mathbf{k})$ is given by one-particle irreducible diagrams. The asymptotic behavior in Eq. (2.12) implies that the small-$\mathbf{k}$ behavior of $\langle\tilde{G}\rangle$ is given by

$$\kappa_e=\kappa_0-\frac{d}{dk^2}\Sigma(\mathbf{k})\bigg|_{\mathbf{k}=0}. \tag{3.4}$$

The Feynman rules for the diagrammatic perturbation expansion are as follows

(i) The wave vector is conserved at each vertex.

(ii) Each full line carries a factor of $1/k^2$.

(iii) The wave vector is integrated around closed loops with a factor $dq/(2\pi)^3$.

(iv) The primitive vertex $\mathbf{V}_i(\mathbf{k}',\mathbf{k})$, whose diagrammatic representation is shown in Fig. 1(a), is given by $\mathbf{V}_i(\mathbf{k}',\mathbf{k})=ik_i'$.

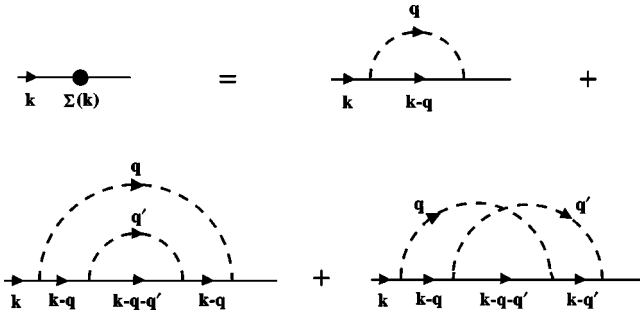(v) Each internal dotted line carries a factor

FIG. 2. The graphs that contribute to two-loop simple perturbation theory for $\tilde{G}(\mathbf{k})$.

$$F_{ij}(\mathbf{k}) = \Phi(\mathbf{k})(k^2 \delta_{ij} - k_i k_j) + \Psi(k) i \epsilon_{imj} k_m. \quad (3.5)$$

In what follows we use the explicit spectra

$$\Phi(\mathbf{k}) = \frac{(2\pi)^{3/2}}{6k_0^2} u_0^2 e^{-k^2/2k_0^2},$$

$$\Psi(\mathbf{k}) = \lambda k \Phi(\mathbf{k}), \quad (3.6)$$

where $\lambda = \sin 2\psi$.

The simple two-loop calculation for κ_e gives the result

$$\kappa_e = \kappa_0 \left(1 + \frac{1}{9} \frac{u_0^2}{\kappa_0^2 k_0^2} + (0.0059\lambda^2 - 0.00884) \frac{u_0^4}{\kappa_0^4 k_0^4} \right). \quad (3.7)$$

The diagrams contributing to this order are shown in Fig. 2. The two-loop integrals were done numerically.

The effect of helicity is not seen until second order. This is evident from the explicit expressions for the diagrams, but is also easily understood because the effect of helicity on κ_e cannot depend on the sign of λ. Hence the graphs with a nonvanishing contribution from the helicity must contain an even number of internal velocity correlators (dotted lines). Clearly, this approach is not applicable to the limit $\kappa_0 \rightarrow 0$ in which we are interested, but a self-consistent method will allow the model to be perturbatively analyzed in this limit; this is described in Sec. IV.

IV. SELF-CONSISTENT METHODS

A self-consistent treatment performs a resummation of an infinite subset of diagrams which gives a continuation of the perturbation theory beyond its normal radius of convergence. The approach is not unique, but depends on how the effective low energy theory is parametrized, and which quantities are treated self-consistently. A successful result will depend on how well the method captures the dominant effects in this way.

We first discuss the simplest approach which treats only κ_e self-consistently. At two loops this gives an excellent fit for κ_e when $\lambda = 0$, but fails for $\lambda \neq 0$. We then generalize the method, and show that we can qualitatively explain the large enhancement in κ_e due to helicity although the approach is still quantitatively deficient. Further generalizations are discussed but have not yet been carried out.
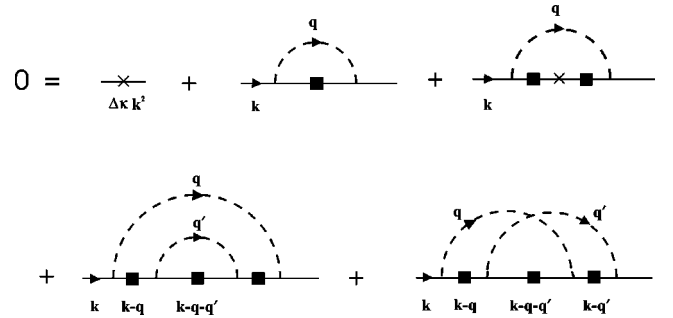

FIG. 3. The perturbation expansion to two loops of the self-consistent relation for κ_e.

A. Self-consistency in κ_e

To generate the self-consistent perturbation series in κ_e, Eq. (3.1) for $G(\mathbf{x})$ is formally rearranged to become

$$\kappa_e \nabla^2 G - \Delta\kappa \nabla^2 G - \mathbf{u} \cdot \nabla G = -\delta(\mathbf{x}), \quad (4.1)$$

where $\Delta\kappa = \kappa_e - \kappa_0$. The second term is a counterterm which is included as a part of the perturbation. It is formally of first order in the expansion parameter, which allows the expansion for κ_e to be constructed to a consistent order. The self-consistent perturbation series is generated by iterating

$$\tilde{G}(\mathbf{k}) = \frac{1}{\kappa_e k^2} + \frac{1}{\kappa_e k^2} \int \frac{d\mathbf{q}}{(2\pi)^3} [i(\mathbf{k} - \mathbf{q}) \cdot \tilde{\mathbf{u}}(q)$$

$$- \Delta\kappa \delta(\mathbf{q})(\mathbf{k} - \mathbf{q})^2] \tilde{G}(\mathbf{k} - \mathbf{q}). \quad (4.2)$$

This equation can be rewritten as an equation for $\Delta\kappa$, and its diagrammatic representation up to two loops is shown in Fig. 3(a). Since κ_e is not renormalized from the tree-level value, we have the self-consistency condition

$$\left. \frac{d}{dk^2} \Sigma(\mathbf{k}) \right|_{\mathbf{k}=0} = 0. \quad (4.3)$$

To Nth order in $u_0^2/\kappa_e^2 k_0^2$, it is always possible to write this condition in the forms

$$\kappa_e = \kappa_0 + \kappa_e F_N(\kappa_e, \lambda),$$

$$F_N(\kappa_e, \lambda) = \sum_{n=1}^{N} g_n(\lambda) \left(\frac{u_0^2}{\kappa_e^2 k_0^2} \right)^n. \quad (4.4)$$

From now on we set $u_0 = 1$ and $k_0 = 1$ and, using the velocity-field spectrum given in Sec. II, we find the two-loop self-consistent expression for κ_e:

$$(\kappa_e - \kappa_0) \left(1 - \frac{1}{9\kappa_e^2} \right) = \kappa_e \left(\frac{1}{9\kappa_e^2} + \frac{1}{\kappa_e^4} [0.0059\lambda^2 - 0.00884] \right). \quad (4.5)$$

This result can be re-expressed in the form of Eq. (4.9) to become

$$\kappa_e = \kappa_0 + \kappa_e \left(\frac{1}{9\kappa_e^2} + \frac{0.0035 + 0.0059\lambda^2}{\kappa_e^4} \right). \qquad (4.6)$$

We show the two-loop self-consistent prediction for κ_e compared with data in Figs. 7–11. In Figs. 7, 8, and 9, κ_e is plotted against κ_0 for fixed $l = 0.0$, 0.4, and 1.0 and in Figs. 10 and 11 κ_e is plotted against λ for fixed $\kappa_0 = 0.0$ and 0.2. As should be expected, we see from Figs. 8 and 9 that the agreement between theory and simulation is acceptable for a value of κ_0 that is large enough. This is simply because the large molecular diffusivity swamps all other effects. However, there is a large disagreement for small κ_0 which is most marked for $\kappa_0 = 0$. The prediction for κ_e behaves like $O(\lambda^2)$, and for κ_0 changes from $\kappa_e = 0.3697$ at $\lambda = 0$ to $\kappa_e = 0.4090$ at $\lambda = 1$: an increase of 10%. In contrast, the simulation gives $\kappa_e = 0.3705(1)$ and $\kappa_e = 0.8018(7)$, respectively, at these two values of λ: an increase of more than a factor of 2. From the simulation for κ_0 small enough we find that κ_e as a function of λ is strongly in disagreement with the slow polynomial behavior in λ predicted by self-consistent perturbation theory. This effect was first observed in Ref. [4] and has remained unexplained.

In addition, in Fig. 9 we observe a marked dip in the data at fixed $\lambda = 1$ for κ_e versus κ_0 at about $\kappa_0 = 0.2$. The major feature is that κ_e rises rapidly with λ at $\kappa_0 = 0$, whereas the effect for $\kappa_0 \geq 0.2$ is much less strong: the dip is not a lowering of the curve as λ increases at $\kappa_0 = 0.2$, but rather a rapid rise with λ at $\kappa_0 = 0$. The self-consistent prediction of this section does not predict a dip of any kind.

B. A more general approach

In this section we propose an explanation of the enhancement of κ_e by helicity in the flow. The technique is presented in detail at the one-loop level and the extension to the two-loop level is then given.

The philosophy is to suggest an effective, low-wave-vector diffusion equation obeyed by the smoothed distribution function. Because the wave vector is small it is assumed that the equation can be limited to at most two spatial derivatives. The shortcomings of this assertion are discussed later. We propose the equation

$$\frac{d\Theta}{dt} = \kappa_0 \nabla^2 \Theta - \alpha_R \mathbf{u} \cdot \boldsymbol{\nabla} \Theta - \beta_R \boldsymbol{\omega} \cdot \boldsymbol{\nabla} \Theta, \qquad (4.7)$$

where $\boldsymbol{\omega}$ is the vorticity and α_R and β_R are coupling constants which must be determined self-consistently. The bare values of these couplings, α_0 and β_0, define the original diffusion equation. From Eq. (2.6) we see that in our case $\alpha_0 = 1$ and $\beta_0 = 0$, but the analysis may be applied for general values of α_0 and β_0. Equation (4.7) is equivalent to renormalizing the velocity field to $\mathbf{u}_R = \alpha_R \mathbf{u} + \beta_R \boldsymbol{\omega}$. It will turn out that α is not renormalized, and so the self-consistency conditions are applied only to determine κ_e and β_R. To this end the equation for $G(\mathbf{x})$ is taken to be

$$\kappa_e \nabla^2 G - \Delta\kappa \nabla^2 G - \alpha_0 \mathbf{u} \cdot \boldsymbol{\nabla} G - \beta_R \boldsymbol{\omega} \cdot \boldsymbol{\nabla} G + \Delta\beta \boldsymbol{\omega} \cdot \boldsymbol{\nabla} G$$
$$= -\delta(\mathbf{x}), \qquad (4.8)$$

where, as before, $\Delta\kappa = \kappa_e - \kappa_0$ and $\Delta\beta = \beta_R - \beta_0$. The rules for perturbation theory are the same as given in Sec. III, with the following additional rules

(vi) The primitive vertex $\mathbf{W}_i(\mathbf{k}', \mathbf{k})$ associated with the vorticity and whose diagrammatic representation is shown in Fig. 1(b), is given by $\mathbf{W}_i(\mathbf{k}', \mathbf{k}) = (\mathbf{k}' \times \mathbf{k})_i$.

(vii) For each vertex of type $\mathbf{V}_i$ there is a factor of α_R, and for each vertex of type $\mathbf{W}_i$ a factor of β_R.

The self-consistent equations are given by setting the next renormalizations of κ_e and β_R to zero in perturbation theory. This gives two equations which simultaneously determine κ_e, α_R, and β_R in terms of the bare parameters κ_0, α_0, and β_0. It is convenient to define a general vertex $\mathbf{U}_i(\mathbf{k}', \mathbf{k})$ of the form

$$\mathbf{U}_i(\mathbf{k}', \mathbf{k}) = iV(\mathbf{k}', \mathbf{k})\mathbf{k}_i' + W(\mathbf{k}', \mathbf{k})(\mathbf{k}' \times \mathbf{k})_i, \qquad (4.9)$$

where the form factors V and W are scalar functions of $\mathbf{k}$ and $\mathbf{k}'$. The bare vertex U_i^0 is defined by $V^0 = \alpha_0$ and $W^0 = \beta_0$. There is no independent form-factor coefficient proportional to $\mathbf{k}_i$ in this expansion, since the velocity field is incompressible. The diagrammatic representation of $\mathbf{U}_i^0$ is shown in Figs. 1(c) and 1(d), where the bare vertex is represented by an open circle while the renormalized vertex additionally carries an inset letter R. Likewise, the general expression for $\langle \tilde{G}(\mathbf{k}) \rangle$ can be defined as

$$\langle \tilde{G}(\mathbf{k}) \rangle = \frac{1}{k^2 [\kappa_0 + \Omega(k^2)]}. \qquad (4.10)$$

To two loops the self-consistent relationships that hold between diagrams are shown in Fig. 5.

We are interested in the low-wave-number properties of the theory, and we use the approximations

$$\Omega(\mathbf{k}^2) = (\kappa_e - \kappa_0) + O(k^2),$$

$$V^R = \alpha_R + O(\mathbf{k}^2, \mathbf{k}'^2, \mathbf{k} \cdot \mathbf{k}'),$$

$$W^R = \beta_R + O(\mathbf{k}^2, \mathbf{k}'^2, \mathbf{k} \cdot \mathbf{k}'). \qquad (4.11)$$

These approximations are consistent with the form considered for the effective equation governing the dispersal [Eq. (4.7)], since the renormalized couplings, α_R and β_R, are given respectively by the coefficients of $\mathbf{k}_i'$ and $(\mathbf{k}' \times \mathbf{k})_i$ in the expansion of $\mathbf{U}_i$. To include higher powers of $\mathbf{k}$ and $\mathbf{k}'$ would, for consistency, require terms involving $\mathbf{u}$ and $\boldsymbol{\omega}$ in Eq. (4.7) with higher powers of $\boldsymbol{\nabla}$. In principle, a functional self-consistent formalism could then be set up for $\Omega(\mathbf{k})$ and $U_i(\mathbf{k}', \mathbf{k})$ treating them respectively as a vector and matrices in wave-number space. However, this is a further generalization that we have not yet pursued, because the amount of computing effort required to determine them numerically is prohibitive. In the present case we are interested only in the low-wave-vector behavior of these functions, and then the
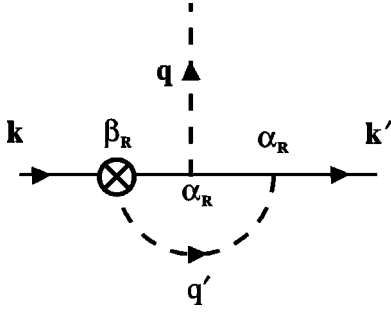
FIG. 4. An example of the kind of vertex graph that must be evaluated in the solution of equations shown in Fig. 5, once the approximation for $\mathbf{U}^R$ given in Eq. (4.11) and shown in Fig. 1 is used. This graph is labeled $T_{\beta\alpha\alpha}$.

self-consistent equations are determined by asserting the self-consistency in the limit $\mathbf{k}',\mathbf{k}\rightarrow\mathbf{0}$ and using Eq. (4.11).

The calculation is now straightforward but tedious. All loop integrals are approximated by their lowest nonzero power in $(\mathbf{k},\mathbf{k}')$, and their contribution to the renormalization of the relevant coupling constant is read off. It suffices to give some examples which indicate how the full result is obtained, and to this end we first analyze the one-loop approximation to the self-consistent equations in detail. The first observation is that α is not renormalized, i.e., $\alpha_R=\alpha_0$. We give one example indicating how this comes about. The graphs are labeled by couplings corresponding to the types of vertex they contain, and the label is ordered in the same order that they occur in the graph. We consider the contribution shown in Fig. 4 to the vertex renormalization, and will concentrate on the part proportional to $\mathbf{k}'$. The value of this graph is

$$T_{\beta\alpha\alpha}=\alpha_R^2\beta_R\int\frac{d\mathbf{q}}{(2\pi)^3}\frac{\epsilon_{lmn}\mathbf{k}_m\mathbf{q}_n(\mathbf{k}'-\mathbf{q})_p\cdot\mathbf{k}_i'F_{lp}(\mathbf{q})}{\kappa_e(\mathbf{k}-\mathbf{q})^2\kappa_e(\mathbf{k}'-\mathbf{q})^2}.$$

(4.12)

The approximations of Eq. (4.11) have been implemented. Only the helical part of $F_{ij}(\mathbf{q})$ contributes, and we find the result

$$T_{\beta\alpha\alpha}=\frac{\alpha_R^2\beta_R\lambda}{\kappa_e^2}ik_i'\int\frac{dq}{(2\pi)^3}$$

$$\times\frac{\epsilon_{lmn}\mathbf{k}_m\cdot\mathbf{q}_n(\mathbf{k}'-\mathbf{q})_p\cdot q\epsilon_{lpq}\mathbf{q}_q\Phi(\mathbf{q})}{(\mathbf{k}-\mathbf{q})^2(\mathbf{k}'-\mathbf{q})^2}$$

$$=\frac{\alpha_R^2\beta_R\lambda}{\kappa_e^2}ik_i'\int\frac{dq}{(2\pi)^3}\frac{(\mathbf{k}\cdot\mathbf{k}'q^2-\mathbf{k}\cdot\mathbf{q}k'\cdot\mathbf{q})q\Phi(\mathbf{q})}{(\mathbf{k}-\mathbf{q})^2(\mathbf{k}'-\mathbf{q})^2}.$$

(4.13)

Clearly the contribution to V is $O(\mathbf{k}\cdot\mathbf{k}')$ and so α is not renormalized. All contributions to V are similarly of higher order and the result is that $\alpha_R=\alpha_0$.

The coupling β is renormalized when $\lambda\neq0$. The calculation follows a similar path to that used in the analysis of the renormalization of α. Again we show one calculation explic-

itly and consider the contribution to $W(\mathbf{k},\mathbf{k}')$ by calculating the coefficient of $(\mathbf{k}'\times\mathbf{k})$ in $T_{\alpha\alpha\alpha}$:

$$T_{\alpha\alpha\alpha}=-i\frac{\alpha_R^3}{\kappa_e^2}\int\frac{d\mathbf{q}}{(2\pi)^3}\frac{(\mathbf{k}-\mathbf{q})_l\cdot(\mathbf{k}'-\mathbf{q})_nF_{ln}(\mathbf{q})}{(\mathbf{k}-\mathbf{q})^2(\mathbf{k}'-\mathbf{q})^2}.$$

(4.14)

The contribution proportional to $(\mathbf{k}'\times\mathbf{k})$ comes only from the helical part of $F_{ln}(q)$ and so the relevant term is

$$T_{\alpha\alpha\alpha}\sim\frac{\alpha_R^3\lambda}{\kappa_e^2}\int\frac{d\mathbf{q}}{(2\pi)^3}\frac{\epsilon_{lnp}\mathbf{k}_l\cdot\mathbf{k}_n'\mathbf{q}_p\cdot\mathbf{q}_mq\Phi(\mathbf{q})}{(\mathbf{k}-\mathbf{q})^2(\mathbf{k}'-\mathbf{q})^2}.$$

(4.15)

Hence we find the contribution $\delta\beta_R$ to the renormalization of β from $T_{\alpha\alpha\alpha}$ to be

$$\delta\beta_R=-\frac{\alpha^3\lambda}{6\pi^3\kappa_e^2}\int dqq^\Phi(\mathbf{q}).$$

(4.16)

The renormalization of β_R is expressed in terms of three integrals:

$$I_n=\frac{1}{6\pi^3}\int dqq^n\Phi(\mathbf{q}),\quad n=1,2,3.$$

(4.17)

After evaluating all the relevant graphs the self-consistent equations are

$$\alpha_R-\alpha_0=0,$$

$$\beta_0-\beta_R+(\alpha_R^3\lambda I_1+2\alpha_R^2\beta_RI_2+\alpha_R\beta_R^2\lambda I_3)=0.\quad(4.18)$$

The approximate equation for $\widetilde{G}(\mathbf{k})$ is given by the equation for $\Sigma(\mathbf{k})$ in terms of the one-particle irreducible graphs in Fig. 5 at one-loop order. Because we are using a low-wave-number approximation, this reduces to substituting the expression for the renormalized vertex $\mathbf{U}_i(\mathbf{k}',\mathbf{k})$ given in Eqs. (4.9) and (4.18) into the one-loop diagram for $\Sigma(\mathbf{k})$ in Fig. 5. We analyze the one-loop self-energy graph and keep only the term proportional to k^2. In obvious notation this gives the results

$$T_{\alpha\alpha}\sim-\frac{2\alpha_R^2}{\kappa_e}I_2,\quad T_{\beta\alpha}\sim\frac{2\alpha_R\beta_R\lambda}{\kappa_e}I_3.$$

(4.19)

Using the spectra in Eq. (3.6), Eqs. (4.18) and (4.19) for the one-loop self-consistent conditions become

$$\Delta\alpha\equiv\alpha_R-\alpha_0=0,\quad-\Delta\beta+\frac{B_1}{\kappa_e^2}=0,\quad\Delta\kappa+\frac{C_1}{\kappa_e}=0.$$
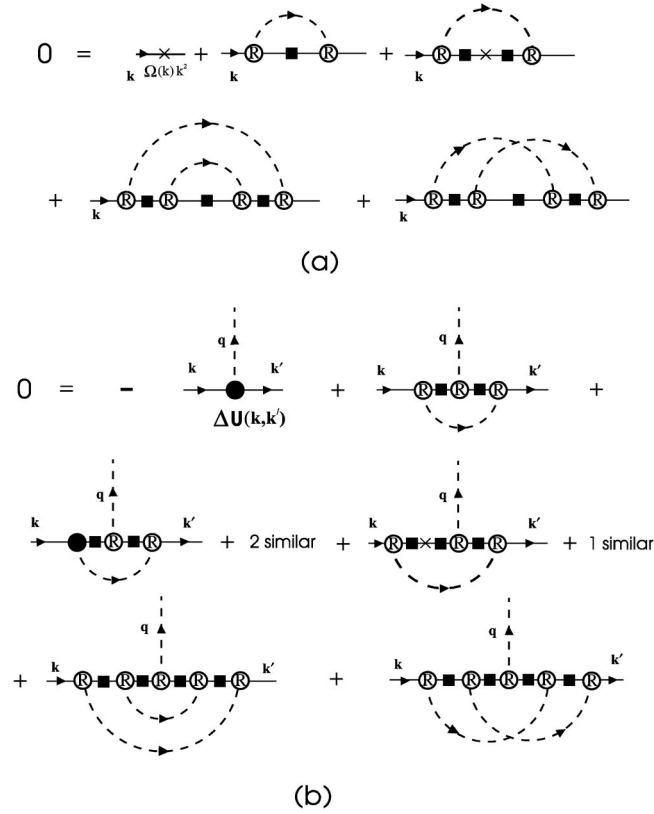
(4.20)

where

FIG. 5. The perturbation expansion to two loops of the general self-consistent condition relating the self-energy $\Sigma(\kappa)$ and vertex $\mathbf{U}^R(\kappa,\mathbf{k}')$ functions. The vertex function is represented by the circle with inset and R, the full Green function by $\tilde{G}(\mathbf{k})$ by the filled box; $\Delta\mathbf{U}=\mathbf{U}^R-\mathbf{U}^0$.

$$B_1=\frac{1}{18}\left(2\alpha_R^2\beta_R+2\sqrt{\frac{2}{\pi}}\,\alpha_R\beta_R^2\lambda+\sqrt{\frac{2}{\pi}}\,\alpha_R^3\lambda\right),$$

$$C_1=-\frac{1}{9}\left(\alpha_R^2+4\sqrt{\frac{2}{\pi}}\,\alpha_R\beta_R\lambda+3\beta_R^2\right). \tag{4.21}$$

From these equations it is clear that no renormalization occurs if there is no pseudoscalar or axial-vector quantity in the problem: if $\beta_0=\lambda=0$, then the problem reduces to the one-loop self-consistent analysis presented in Sec. IV A. However, if either β_0 or λ are nonzero then β is renormalized and the effect on κ_e is encoded in Eq. (4.20). In our case we set $\alpha_R=\alpha_0=1$, $\beta_0=0$, and $\lambda\neq0$. Equations (4.20) and (4.21) then give

$$3\sqrt{\frac{\pi}{2}}\,\beta^3+3\beta_R^2\lambda+9\sqrt{\frac{\pi}{2}}\,\kappa_e\kappa_0\beta_R-\frac{\lambda}{2}=0.$$

$$\kappa_e=\kappa_0+\frac{1}{9\kappa_e}\left(\alpha_R^2+4\sqrt{\frac{2}{\pi}}\,\alpha_R\beta_R\lambda+3\beta_R^2\right). \tag{4.22}$$

For small λ and $\kappa_0=0$, we deduce that

$$\beta\sim\left(\frac{1}{18\pi}\right)^{1/6}\lambda^{1/3}\Rightarrow\kappa_e\sim\frac{1}{3}+\frac{1}{2}\left(\frac{1}{18\pi}\right)^{1/3}\lambda^{2/3}. \tag{4.23}$$

The data for κ_e versus λ for $\kappa_0=0$ is shown in Fig. 10, and we see that for small λ the simulation results are not compatible with $\lambda^{2/3}$ behavior. We shall see below that this is not rectified in the two-loop self-consistent calculation. However, in this one-loop calculation there is a considerable enhancement in the dependence of κ_e on λ, whereas in the self-consistent calculation of Sec. IV A, in which the generation of the new vertex coupled to the vorticity $\boldsymbol{\omega}$ was not included, there is no effect at all at one-loop order and only a mild effect at two-loop order. Equation (4.22) can be solved numerically. For example, for $\kappa_0=0$ and $\lambda=1$, we find $\beta_R=0.3456$, and the effective velocity field is predicted to be

$$\mathbf{u}_R=\mathbf{u}+\beta_R\boldsymbol{\omega}, \tag{4.24}$$

which clearly leads to an enhanced effective diffusivity $\kappa_e=0.5207$, compared with $\kappa_e=0.4090$ from the two-loop calculation of Sec. III. We believe that we have qualitatively captured the mechanism responsible for the enhancement of the effective diffusivity by helicity.

The one-loop calculation is limited because it is not accurate at $\lambda=0$, unlike the two-loop calculation. We have investigated the two-loop extension of the self-consistent approach when the new vertex with coupling β is included. This is more involved, and the integrals were done numerically. We present the final results below.

The two-loop self-consistent equations are

$$\Delta\kappa+\frac{C_1}{\kappa_e}-\Delta\beta\frac{1}{\kappa_e}\frac{\partial C_1}{\partial\beta}+\frac{1}{\kappa_e^3}(C_2-C_1^2)=0,$$

$$-\Delta\beta+\frac{B_1}{\kappa_e^2}+2\frac{\Delta\kappa}{\kappa_e^3}B_1-\Delta\beta\frac{1}{\kappa_e^2}\frac{\partial B_1}{\partial\beta}+\frac{B_2}{\kappa_e^4}=0, \tag{4.25}$$

where B_1 and C_1 are given in Eq. (4.21), and B_2 and C_2 are evaluated numerically to be ($\alpha_R=\alpha_0=1$)

$$B_2=-(0.0047\lambda+0.0095\beta+0.0180\beta\lambda^2+0.0644\beta^2\lambda$$
$$+0.0423\beta^3+0.0252\beta^3\lambda^2+0.0287\beta^4\lambda),$$

$$C_2=0.0088-0.0034\lambda^2-0.0165\beta\lambda-0.0315\beta^2$$
$$-0.0110\beta^2\lambda^2-0.0514\beta^3\lambda+0.0090\beta^4-0.0337\beta^4\lambda^2. \tag{4.26}$$

Equations (4.25) can be rearranged to give

$$\Delta\kappa+\frac{C_1}{\kappa_e^2}+\frac{1}{\kappa_e^3}\left(C_2-C_1^2-B_1\frac{\partial C_1}{\partial\beta}\right)=0,$$

$$-\Delta\beta+\frac{B_1}{\kappa_e^2}+\frac{1}{\kappa_e^4}\left(B_2-2B_1C_1-B_1\frac{\partial B_1}{\partial\beta}\right)=0. \tag{4.27}$$

We shall set $\beta_0=0$ from now on. These equations contain the accurate two-loop self-consistent result which fits the data for all κ_0 at $\lambda=0$. For $\lambda\neq0$ these equations are solved numerically and the results are compared with simulation data in Figs. 7–11 As in the one-loop case, the behavior for small λ is clearly incorrect, and there is no quantitative
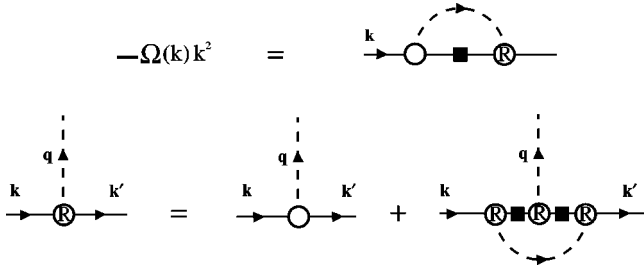
FIG. 6. The integral Hartree-Fock equations for $\Omega(k)$ and $\mathbf{U}^R$ in terms of the general vertices $\mathbf{U}^O$ and $\mathbf{U}^R$. The full Green function $\widetilde{G}(\mathbf{k})$ is denoted by the filled box. The equation for $\Omega(\mathbf{k})$ is correct to all loop orders, but the equation for $\mathbf{U}^R$ is correct to one-loop order only

FIG. 7. κ_e vs $\kappa 0$ for fixed helicity $\lambda = 0.0$. The simulation data are shown ($\bigcirc$) to be compared with the predictions of two-loop self-consistent perturbation theory (solid line), the Hartree-Fock calculation (long-dashed line), the renormalization group (dashed line) and ordinary perturbation theory (dot-dashed line).

agreement with the data. However, there is a clear enhancement of κ_e due to the inclusion of the vorticity vertex and associated coupling β, and for $\lambda = 1.0$ we find $\kappa_e = 0.5959$. This mechanism for enhancing turbulent diffusion cannot be obviously deduced from perturbative considerations. It arises from a resummation of diagrams which give an expression that analytically continues between the regions where $\lambda^2 \ll u_0^2/\kappa_0^4 k_0^4$ and $\lambda^2 \gg u_0^2/\kappa_0^4 k_0^4$. The effective diffusivity in the former region is well predicted by perturbation theory, but not so for parameters in the latter region. Although quantitative agreement is not good, the important point is that a mechanism has been discovered which gives a strong enhancement to the value of κ_e for nonzero λ even in the one-loop approximation, whereas in the self-consistent theory for κ_e alone, discussed in Sec. III, there is no effect of helicity at all on the value of κ_e at one-loop order. The obvious reason for the discrepancy in this approach is that the approximations made are much too crude. A more refined calculation would use a functional self-consistent method for $\mathbf{U}_i(\mathbf{k}', \mathbf{k})$ [Eq. (4.9)] and $\Omega(k^2)$ [Eq. (4.10)]. Although a computationally formidable task, this is likely to encode the correct behavior much more accurately than does our low-wavenumber approximation. The origin of the dip in Fig. 9 in the curve κ_e versus κ_0 for $\lambda = 1$ is unexplained by the theory presented so far.

V. FUNCTIONAL HARTREE-FOCK METHOD

This approach goes some way toward including effects omitted in the low-wave-number approximation. The version presented here is deficient in that the prediction for κ_e, when $\kappa_0 = \lambda = 0$, is not as accurate as the two-loop self-consistent approach, but the advantage is that $\Omega(k^2)$, Eq. (4.10), is treated as a function to be determined self-consistently by the Hartree-Fock equations. The vertices are still treated in the low-wave-number approximation, and, as in Sec. IV, they are parametrized by α and β.

The integral equation to be satisfied by $\Omega(k^2)$ and the one-loop equation satisfied by the vertex function, which is the same as the one-loop self-consistent equation, are shown in Fig. 6. Note that, unlike the self-consistent calculation of Sec. IV, only one of the vertices in the one-loop self-energy is replaced by the full vertex, since this gives the correct
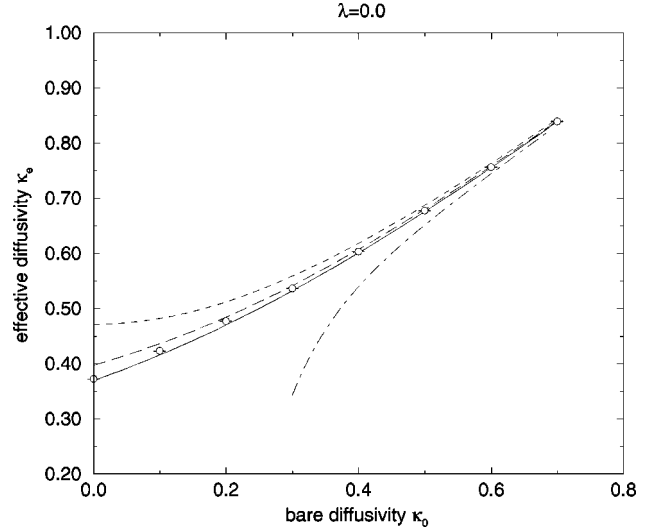
counting of diagrams when the equations are iterated. The self-consistent case is different because the augmented vertex is already present in the perturbation theory, and corrections are implemented by counter terms. The approximation for the vertices in Eq. (4.11) is used and β is determined using Eq. (4.20):

$$\beta = \beta_0 + \frac{B_1}{\kappa_e^2}, \tag{5.1}$$

where B_1 is given in Eq. (4.21) and using $\kappa_e = \kappa_0 + \Omega(0)$. The Hartree-Fock equation to be satisfied by $\Omega(k^2)$ is then [after some reduction, and using ϕ in Eq. (3.6)],

$$\Omega(k^2) = \frac{1}{k^2} \left[\frac{2}{3\sqrt{2\pi}} e^{-k^2/2} \right.$$

$$\times \int dp \frac{[pk \cosh(pk) - \sinh(pk)]e^{-p^2/2}}{pk[\kappa_0 + \Omega(p^2)]}$$

$$\left. + \beta\lambda \int \frac{d^3p}{(2\pi)^3} \frac{|\mathbf{p}+\mathbf{k}|\phi(|\mathbf{p}+\mathbf{k}|)[k^2 p^2 - (\mathbf{k}\cdot\mathbf{p})^2]}{p^2(\kappa_0 + \Omega(p^2))} \right]. \tag{5.2}$$

These equations are solved by discretizing the wave vector, performing the integrals numerically, and iterating the equations to converge to a solution for $\Omega(k^2)$. The effective diffusivity is then $\kappa_e = \kappa_0 + \Omega(0)$.

The results are shown in Figs. 7–11, where it is clear that while the numerical value predicted at $\kappa_0 = \lambda = 0$ is not accurate, the behavior for small λ is more in keeping with the simulation results. This strengthens our belief that an analysis which treats the propagator and vertex as functions to be determined self-consistently is likely to reproduce the de-
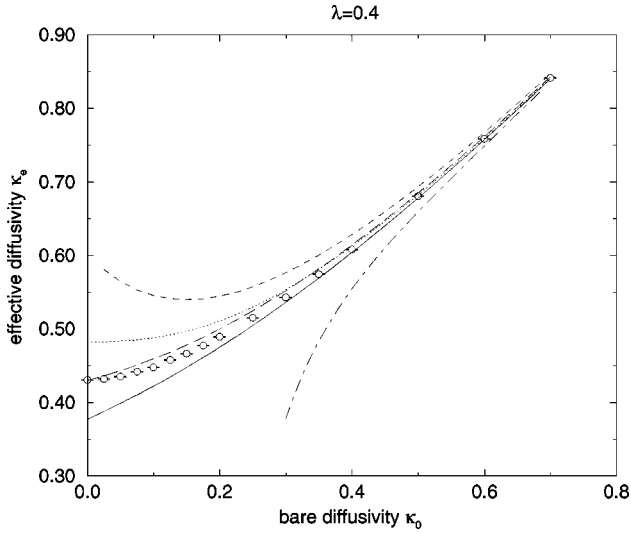
FIG. 8. κ_e vs $\kappa0$ for fixed helicity $\lambda = 0.4$. The simulation data are shown ($\bigcirc$) to be compared with the predictions of two-loop self-consistent perturbation theory in κ_e (solid line), and κ_e, β (dotted line), the Hartree-Fock calculation (long-dashed line), the renormalization group (dashed line), and ordinary perturbation theory (dot-dashed line).

sired properties more accurately. However, at $\kappa_0 = 0$ and $\lambda = 1$ the value predicted is $\kappa_e = 0.5070$, still much less than the simulation value of 0.8018(7).

In principle, the vertex may be treated as a function in the same manner as $\Omega(k^2)$. This is prohibitively expensive in memory and computer time, but might be possible if some simplification of the functional form were implemented. Also, while the equation for $\Omega(k^2)$ is already exact at the one-loop level, that for the vertex is not, and we cannot pre-
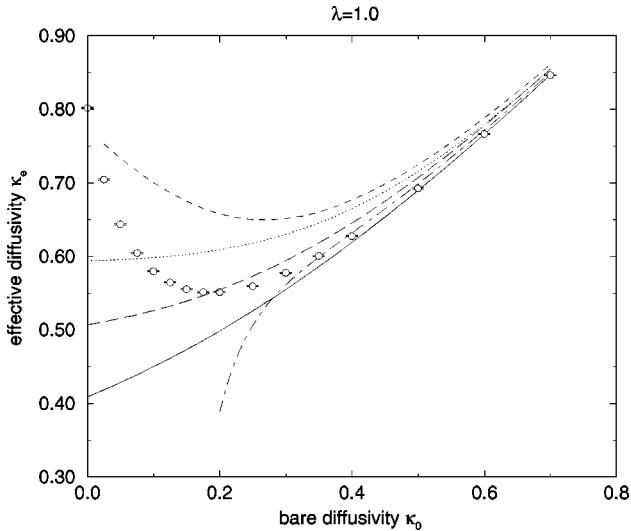

FIG. 9. κ_e vs $\kappa0$ for fixed helicity $\lambda = 1.0$. The simulation data are shown ($\bigcirc$) to be compared with the predictions of two-loop self-consistent perturbation theory in κ_e (solid line) and κ_e, β (dotted line), the Hartree-Fock calculation (long-dashed line), the renormalization group (dashed line), and ordinary perturbation theory (dot-dashed line).
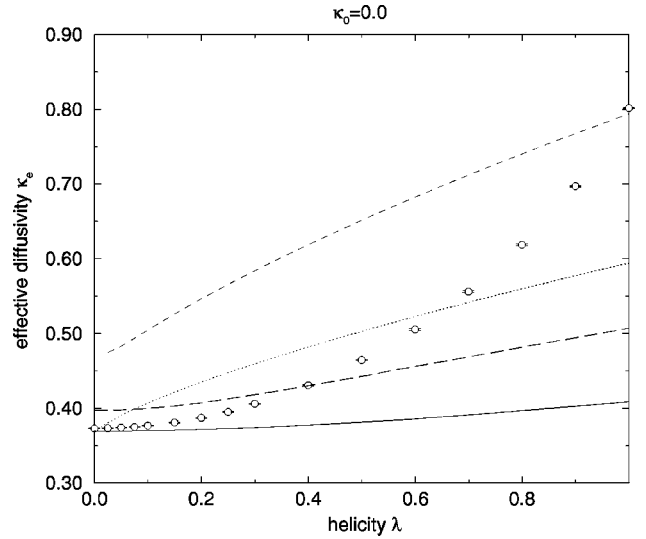

FIG. 10. κ_e vs λ for fixed diffusivity $\kappa_0 = 0.0$. The simulation data are shown ($\bigcirc$) to be compared with the predictions of two-loop self-consistent perturbation theory in κ_e (solid line) and κ_e, β (dotted line), the Hartree-Fock calculation (long-dashed line), and the renormalization group (dashed line).

clude that higher loop corrections might be important. We have not pursued this approach. We note that in this approach, as with those of the previous sections, the marked dip in κ_e as a function of κ_0 for the larger values of λ is not reproduced.

VI. RENORMALIZATION GROUP

In Sec. V we presented an analysis based on the assumption that the large-scale advection is controlled by an effective transport equation dominated by the terms containing only one and two derivatives. This method is related to
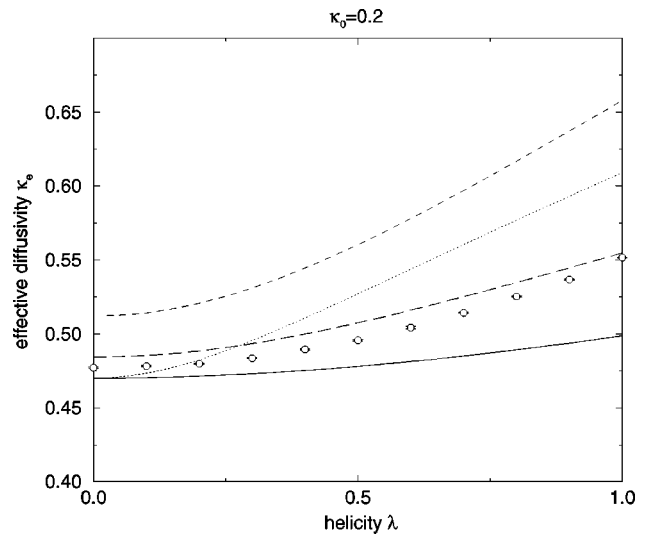

FIG. 11. κ_e vs λ for fixed diffusivity $\kappa_0 = 0.2$. The simulation data are shown ($\bigcirc$) to be compared with the predictions of two-loop self-consistent perturbation theory in κ_e (solid line) and κ_e, β (dotted line), the Hartree-Fock calculation (long-dashed line), and the renormalization group (dashed line).

renormalization group methods which have proved very successful in predicting exponents in critical phenomenon. In the RG approach a large wave-number cutoff Λ is introduced, and advection on scales larger than $L \equiv 2\pi/\Lambda$ is assumed to be described by an effective transport equation, in principle containing terms with an arbitrarily high number of derivatives. The parameters in this equation are functions of Λ in order to account for the effect of advection at scales smaller than L which has been excised. In the limit $\Lambda \to 0$ the effective equation, by dimensional analysis, takes a simple form dominated by terms with few derivatives and with associated effective or ''renormalized'' parameters. In this way the effective equation takes a form similar to that used in Sec. V. There is a difference, however, because any practical application of these schemes requires a drastic truncation of the operator space: this is especially true in the RG method, where it is impossible to compute the flow with changing Λ for very many parameters in the effective transport equation. Unlike the situation in critical phenomena, there are no infrared divergences in the theory, and the notion of a relevant operator is not applicable. It is then a matter of trial and error to determine whether the approach used captures the vital features controlling the flow. The simplest renormalization scheme is to calculate the renormalization to the diffusivity $\kappa(\Lambda)$ and to the vertex associated with the coupling of the random field or externally applied drift. In the case of gradient flows, we demonstrated in Ref. [7] that this scheme yields exact results in one and two dimensions and an extremely accurate, although not exact, result in three dimensions. It is, in general, much harder to calculate the renormalized parameters such as κ_e than the associated exponents, and so the success in Ref. [7] suggests that some insight may be gained using RG methods in other similar problems.

In this section we present a RG calculation of κ_e. The vertex renormalization is done but multiple vertex renormalization is neglected, which means that the renormalized velocity field remains Gaussian. Consequently, after integrating out the random field down to a wave number Λ, we postulate that the equation for the effective Green function can be approximated, for all Λ, by an equation of the same form as the original one [Eq. (3.1)],

$$\kappa(\Lambda)\nabla^2 G(x,\Lambda) - \mathbf{u}(\mathbf{x},\Lambda)\cdot\nabla G(\mathbf{x},\Lambda) = -\delta(\mathbf{x}), \quad (6.1)$$

where $\kappa(\Lambda)$ is the running renormalized diffusion constant and $\mathbf{u}_\Lambda$ is the renormalized velocity field. Since we renormalize the vertex functionally, the field correlation function will flow under the RG as

$$\langle \widetilde{u}_i(k,\Lambda)\widetilde{u}_j(\mathbf{k}',\Lambda)\rangle = \begin{cases} (2\pi)^3 \delta(\mathbf{k}+\mathbf{k}')F_{ij}(k,\Lambda), & |\mathbf{k}|<\Lambda \\ 0, & |\mathbf{k}|>\Lambda, \end{cases}$$

$$(6.2)$$

where

$$F_{ij}(\mathbf{k},\Lambda) = \Phi(\mathbf{k},\Lambda)(k^2\delta_{ij} - k_ik_j) + \Psi(\mathbf{k},\Lambda)i\epsilon_{imj}k_m. \quad (6.3)$$

One finds that the renormalized field is still incompressible. We shall compute the flow equations for $\kappa(\Lambda)$, $\Phi(k,\Lambda)$, and $\Psi(k,\Lambda)$ as Λ varies.

The change in $\kappa(\Lambda)$ on integrating out wave vectors in the shell $(\Lambda,\Lambda-\delta\Lambda)$ is

$$\delta_\kappa(\Lambda) = -\frac{1}{3\pi^2\kappa(\Lambda)}\Lambda^2\Phi(\Lambda,\Lambda)\delta\lambda. \quad (6.4)$$

If one calculates the vertex renormalization, and treats it as an addition to the random field one finds

$$i\mathbf{k}\cdot\delta\widetilde{\mathbf{u}}(\mathbf{q},\Lambda) + O(k^2)$$

$$= -\frac{i}{(2\pi)^3}\int_{\Lambda-\delta\Lambda}^{\Lambda}\frac{F_{ij}(\mathbf{q}',\Lambda)k_iq_jq_k'\widetilde{u}_k(\mathbf{q},\Lambda)}{\kappa^2(\Lambda)q'^2(\mathbf{q}+\mathbf{q}')^2}d\mathbf{q}', \quad (6.5)$$

where we have only kept the vertex term to lowest order in k, as it is only this term that contributes to the one-loop diffusivity renormalization. In addition, if one assumes that it is the low-wave-number (long distance) renormalization of the velocity field which is important for the effective diffusivity, one finds, to lowest order in q,

$$\delta\widetilde{u}_i(q,\Lambda) \approx -\frac{1}{(2\pi)^3\kappa^2(\Lambda)}q_j\widetilde{u}_k(q,\Lambda)$$

$$\times \int_{\Lambda-\delta\Lambda}^{\Lambda}\frac{F_{ij}(\mathbf{q}'\Lambda)q_k'}{q'^4}d\mathbf{q}'. \quad (6.6)$$

In the case where no helicity is present we see that the vertex is not renormalized. However (as pointed out Sec. III), while the helicity does not contribute to the diffusivity renormalization at a one-loop level it renormalizes the velocity field. The renormalization is zero at order 0 in q but has an order 1 effect:

$$\delta\widetilde{u}_i(\mathbf{q},\Lambda) \approx -\frac{1}{6\pi^2\kappa^2(\Lambda)}\epsilon_{ijk}q_j\widetilde{u}_i(\mathbf{q},\Lambda)\Psi(\Lambda,\Lambda)\delta\Lambda,$$

$$(6.7)$$

In real space therefore, the renormalization is of the form

$$\mathbf{u}\to\mathbf{u} + \delta\Lambda\beta(\Lambda)\nabla\times\mathbf{u}. \quad (6.8)$$

Using the renormalization of $\widetilde{\mathbf{u}}$, one may compute the flow of F_{ij}, and thus Φ and Ψ, to obtain the one-loop functional RG equations:

$$\frac{\partial\kappa}{\partial\Lambda} = -\frac{1}{3\pi^2\kappa(\Lambda)}\Lambda^2\Phi(\Lambda,\Lambda),$$

$$\frac{\partial\Phi(q,\Lambda)}{\partial\Lambda} = -\frac{1}{3\pi^2\kappa^2(\Lambda)}\Psi(q,\Lambda)\Psi(\Lambda,\Lambda),$$

$$(6.9)$$

$$\frac{\partial\Psi(q,\Lambda)}{\partial\Lambda} = -\frac{1}{3\pi^2\kappa^2(\Lambda)}q^2\Phi(q,\Lambda)\Psi(\Lambda,\Lambda)$$

The integration of Eqs. (6.9) is from $\Lambda = \infty$ to 0, with the initial conditions

$$\kappa(\infty) = \kappa_0,$$

$$\Phi(q,\infty) = \Phi(q), \qquad (6.10)$$

$$\Psi(q,\infty) = \Psi(q).$$

When there is no helicity there is no vertex renormalization at the order we are considering, and therefore we may integrate the equations directly to obtain

$$\kappa_e = (\kappa_0^2 + 2u_0^2/9)^{1/2}. \qquad (6.11)$$

This agrees with the one-loop perturbation result, as it should, and in the case $\kappa_0 = 0$ we find that $\kappa_e = \sqrt{2}/3 = 0.47140$, which is quantitatively not very close to the numerically measured result $\kappa_e = 0.3697$. However, the discrepancy is sensitive to the form assumed for the effective diffusion equation. In our case this is given by Eq. (6.1), which is clearly inadequate since **u** is not renormalized when $\lambda = 0$. An improvement can only be made by including terms with higher derivatives of **u**. This is similar to parametrizing the nonhelical form factor V^R of Eq. (4.9) with a function of external momenta rather than approximating it by a constant α_R which is not renormalized. This is a possible avenue of research but we have not yet followed it.

In contrast, for $\lambda \neq 0$, u is renormalized and the effect on κ_e is significant because the helical form factor W^R, Eq. (4.9) is renormalized at low wave number, as parametrized by $\beta(\Lambda)$ above. The RG equations may be integrated numerically, and are compared with simulation in Figs. 7–11. Although the results are not quantitatively accurate, they capture the qualitative behavior seen in the simulations. In particular, the RG predicts the large enhancement as a function of λ seen in the data, and also predicts the dip observed in the graph of κ_e versus κ_0 for sufficiently large λ.

Indeed, the qualitative success of the method suggests that the difficulty in obtaining predictions that are more accurate might lie with the inadequacy of the simple ansatz when applied to the case when $\lambda = 0$. The effect of helicity is nevertheless well captured in this approach, because this effect is dominated by the renormalization of $\beta(\Lambda)$.

A technical point in the numerical integration is that $\kappa_0 = 0 \Rightarrow \kappa(\infty) = 0$, and the evolution equations are ill defined in the limit $\Lambda \to \infty$. This problem is easily rectified by making κ_0 very small but nonzero. The integration procedure is then well defined, and the results are insensitive to the exact value of κ_0 in this case.

We therefore believe that although the renormalization procedure is not quantitatively accurate (as should be expected as it does not give very accurate results in the absence of helicity), it successfully incorporates the underlying mechanism for the enhancement of the diffusivity by helicity at small bare molecular diffusivity.

VII. DISCUSSION AND CONCLUSIONS

In this paper we have studied the problem of turbulent advection of a scalar field by an incompressible flow with helicity λ, $0 \leq \lambda \leq 1.0$, and background molecular diffusivity κ_0. We have performed computer simulations of the advec-

tion for flows with properties described in Eqs. (2.1)–(2.4), and compared the long-range effective parameters describing the time evolution of the scalar field with various schemes of calculation. In particular, we have concentrated on how the effective diffusivity κ_e depends on κ_0 and λ. In earlier work we found a strong anomalous enhancement of κ_e as a function of λ for $\kappa_0 = 0.0$ [4], which was unexplained theoretically, and this is the motivation for the present study. In that earlier work the turbulent velocity field was time dependent, whereas here it is not. This allows for easier calculation while still reproducing the effect.

The important region for discussion can be seen from the simulation data, (Figs. 7–11) to be $\kappa_0 < 0.2$; for larger κ_0 the molecular diffusivity begins to dominate, and not only is the effect of helicity suppressed but also the many schemes of calculation give good approximations for κ_e. For $\lambda = 0.0$ we find that the two-loop self-consistent calculation of κ_e reproduces the simulation data for all κ_0 very closely indeed, as is seen in Fig. 7 and described in Sec. IV. The other schemes also plotted are much less accurate in the region of interest. Ordinary perturbation theory is not convergent in this region and will be discussed no further. The reason why the Hartree-Fock and RG methods are less accurate is that the vertex function $V(\mathbf{k}',\mathbf{k})$ [Eq. (4.9)], is not renormalized for low wave number, which means that the associated coupling α is not renormalized. The Hartree-Fock method at $\lambda = 0$ sums rainbow diagrams, but does not include any diagrams corresponding to a vertex correction, unlike the self-consistent theory. In the self-consistent theory the one-loop prediction for $\kappa_0 = 0$ is $\kappa_e = 1/3$ and the two-loop terms modify this by $\delta\kappa_e \sim 0.04$, of which the two-loop cross diagram in Fig. 3 contributes only 10%, or $\delta\kappa_e \sim 0.004$. In omitting terms similar to this latter one, the Hartree-Fock approximation should therefore not be expected to be too discrepant, and this is seen to be the case. The RG calculation gives a form which must yield the simple one-loop perturbation theory expression at large κ_0, but allows continuation to $\kappa_0 = 0$; this is given in Eq. (6.11). In the case of gradient flows the RG approach is remarkably successful [6], and this is attributed to the fact that in that case the primitive vertex is renormalized at low wave number. The reason for examining schemes alternative to self-consistent methods is that for $\lambda > 0$ agreement between simulation data and theory is poor, and it is necessary to investigate different approaches in order to test different hypotheses for a simple description of the observed anomalous effect.

For $\kappa_0 > 0.2$ all schemes except ordinary perturbation theory begin to show reasonable agreement with the data, and for $\kappa_0 > 0.5$ all schemes clearly reproduce the results. We concentrate on results for $\kappa_0 < 0.2$, and the anomalous enhancement of κ_e by helicity in this region is seen in Fig. 10, where κ_e is plotted against λ for $\kappa_0 = 0$, and is characterized by a rapid rise in κ_e for $\lambda > 0.2$. An alternative aspect is seen in Fig. 9, where κ_e is plotted against κ_0 for $\lambda = 1.0$. The significant dip at $\kappa_0 = 0.2$ is due to the large effect of helicity on κ_e compared with the much reduced effect at $\kappa_0 \sim 0.2$. It has proved very difficult to convincingly explain these features. However, we have been able to suggest mechanisms which show the presence of helicity in the flow

can produce a large change in κ_e from the nonhelical value, and even though these have not yet yielded quantitative predictions they do point toward a reasonable explanation.

The basic idea is to recognize that the effective equation governing the advection should contain terms not present in the original equation. The terms can be thought of as being induced in the low-wave-number effective theory by integrating out higher wave numbers. This may also be viewed as the renormalization of the related vertex functions of the theory corresponding to a selective resummation of diagrams. In our approach we have assumed that a low-wave-number approximation will be valid, and so that such terms will contain a minimum number of derivatives. These ideas can be implemented in different ways and we tried self-consistent, Hartree-Fock, and renormalization group approaches. The self-consistent and Hartree-Fock methods are based on the effective evolution equation (4.7) which corresponds to a low-wave-number enhancement of the flow velocity $u_R = u + \beta_R \omega$, where ω is the vorticity. We performed a two-loop calculation self-consistent in both κ_e and β_R, as described in Eq. (4.25) and Fig. 5. The results show that a strong enhancement in κ_e is predicted, but that the magnitude for $\lambda = 1.0$ and $\kappa_0 = 0.0$ is too small and the form of the dependence of κ_e on λ disagrees with the data. This is particularly true at small λ for $\kappa_0 = 0.0$, where, from Fig. 10 we see that κ_e is only weakly dependent on λ, $\lambda < 0.3$, whereas we predict $\kappa_e \sim a + b\lambda^p$ for fractional p: the one-loop result is $p = 2/3$.

The Hartree-Fock method, shown diagramatically in Fig. 6, computes the complete propagator in terms of $\Omega(k^2)$ [Eq. (4.10)] as a sum of the rainbow diagrams generated from the effective equation (4.7) with β_R given by the one-loop result

$\beta_R = -B_1(\beta_R)/\kappa_e^2$ where $B_1(\beta_R)$ is given in Eq. (4.21) and $\kappa_e = \kappa_0 + \Omega(0)$. A rise in κ_e with λ is predicted, but not one large enough to agree with the data. However, the behavior at small λ is a much slower rise, which is more in keeping with the data than the self-consistent prediction in this region.

The renormalization group method is a different approach in that it considers a running diffusivity $\kappa(\Lambda)$ and velocity field $\mathbf{u}(\mathbf{x}, \Lambda)$ which satisfy $\kappa(\infty) = \kappa_0$, $\kappa(0) = \kappa_e$, and $\mathbf{u}(\mathbf{x}, \Lambda) = \mathbf{u}(\mathbf{x})$. There are three coupled RG flow equations, [see Eq. (6.9)], for $\kappa(\Lambda)$ and the two running spectral functions $\Phi(q, \Lambda), \Psi(q, \Lambda)$ which correspond to the definitions in Eq. (6.3). The important feature of the RG flow equations is that $\kappa(\Lambda)$ appears in the denominators. The numerators are suppressed at large Λ by the spectral functions, and so the major contribution is from intermediate values of Λ: $\Lambda \sim k_0$. This contribution is strongly enhanced for small κ_0, and results in the prediction of the dip structure observed in the data but not predicted by the other methods.

From our investigation we must expect that a proper explanation of the observed effects will require the correct effective equation and the consequent generation of new vertices, but that unlike the $\lambda = 0$ case the low-wave-number approximation will be insufficient since, although an enhancement is predicted for $\lambda \neq 0$ the rapid rise is not reproduced and no dip is observed. The RG method suggests that the main contribution is from wave numbers $k \sim k_0$ supporting this latter conclusion. A successful approach should therefore include more terms in the effective flow equation in combination with an RG approach. The challenge is to obtain accurate results for all λ including $\lambda = 0$ by such a technique. Work in this direction is currently underway.

[1] R. H. Kraichnan, Phys. Fluids **13**, 22 (1970).

[2] R. H. Kraichnan, J. Fluid Mech. **77**, 753 (1976).

[3] R. H. Kraichnan, J. Fluid Mech. **81**, 385 (1977).

[4] I. T. Drummond, S. Duane, and R. R. Horgan, Nucl. Phys. B **220**, 119 (1983).

[5] I. T. Drummond and R. R. Horgan, Phys. Lett. B **321**, 246 (1994).

[6] D. S. Dean, I. T. Drummond, and R. R. Horgan, J. Phys. A **27**, 5135 (1994).

[7] D. S. Dean, I. T. Drummond, and R. R. Horgan, J. Phys. A **28**, 1235 (1995).

[8] R. Phythian and W. D. Curtis, J. Fluid Mech. **89**, 241 (1978).

[9] I. T. Drummond, S. Duane, and R. R. Horgan, J. Fluid Mech. **138**, 75 (1984).